Indian Journal of Chemical Technology
Vol. 31, May 2024, pp. 355-368
DOI: 10.56042/ijct.v31i3.7041

Removal of methyl orange and methylene blue from wastewater by magnetic nanocomposites loaded activated carbon synthesised from walnut shell

Panneerselvam Anitha[1], Arumugam Ramachandran[2], Ramasamy Sudha[3]*, Nataraj Valarmathi[3] & Dharamraj Geetha[4]

[1]Centre for Research, Department of Chemistry, Government College of Engineering, Salem-636 011, Tamil Nadu, India

[2]Department of Chemistry, Government College of Engineering, Tirunelveli-627 007, Tamil Nadu, India

[3]Department of Chemistry, Vivekanandha College of Arts and Sciences for Women (Autonomous), Tiruchengode, Namakkal- 637 205, Tamil Nadu, India

[4]Department of Chemistry, Vivekanandha Arts and Science College for Women, Sankari, Salem- 637 303, Tamil Nadu, India

*Email: drsudha@vicas.org

Received 13 December 2023; accepted 2 April 2024

The novel magnetic nanocomposites activated carbon (MWNSC) has been synthesised from activated carbon (AC), produced from walnut shell through pyrolysis method. This adsorbent has been characterized by FTIR, BET, TEM, SEM and EDX analysis techniques. The effects of various adsorption factors such as pH of the dye solution, contact time, and adsorbent dose have been studied. Adsorption isotherms have been employed to test the experimental data, and the results corresponded well to the Langmuir model, with MO and MB having maximal adsorption capacities of 303.30 and 345.70 mg g^{-1}, respectively. Adsorption kinetics have been studied using pseudo-first-order, pseudo-second-order, Elovich and intraparticle diffusion models, and the experimental results are well-fitted with the pseudo second-order model. According to the dye adsorption's thermodynamics, the process is exothermic, spontaneous, and favourable from a thermodynamic standpoint. The method is applicable to real wastewater samples, with 99 % removal of MO and MB. The outcomes of the present study show that MWNSC is an inexpensive biosorbent that is successfully utilized in removing methyl orange and methylene blue dyes from wastewater.

Keywords: Activated carbon, Adsorption, Dye removal, Magnetic nanocomposite

Introduction

The availability of safe and clean water is a serious issue around the world. Pollutants damage water quality over time and are the source of a broad range of health issues[1]. The primary sources of water pollution are industrial dye effluents such as textiles, leather, cosmetics, and plastics[2]. Dye-polluted water affects aquatic ecosystems and is a major source of public health concerns such as skin irritation, respiratory infections, mental disease, and so on[3]. Among the various organic dyes anionic, cationic, and non-ionic, azo dyes are a broad class of synthetic dyes with azo groups (-N=N-). Azo dyes are highly poisonous, carcinogenic, and teratogenic due to its aromatic rings and -N=N- groups in their structure, along with damaging to the environment and biological life[4,5]. Up to 20% of the azo dyes used in textile companies are eventually dumped to the environment as effluent, producing severe toxicity and mutagenicity in aquatic life and humans[6].

Methyl orange (MO) is a well-known anionic azo dye that is toxic to the environment and biological systems, hence it must be handled gently before being released into the environment[7]. MO is soluble in water and resistant to degradation; removing it from aqueous solutions using present water treatment techniques is complicated. Furthermore, if not properly handled, MO remains in the environment and poses a threat to living beings. Because dyes have mutagenic and carcinogenic properties, their leakage into wastewater has been related to factors that affect human health[8]. Methylene blue (MB) is another most widely utilised dye in the textile industry, and it is used for dyeing and finishing materials. In any case, excessive MB exposure is dangerous to people and marine life since it may create skin sensitivities, sensory system difficulties, and, ultimately, cardiovascular disease[9].

Water pollution is mostly caused by untreated dye effluents that are produced from a variety of sources. There is a technological need for dye effluent treatment systems to safeguard water from contamination. Effective wastewater treatment techniques can result in cleaner, more sustainable growth[10]. Thus, it was

suggested to treat wastewater using various techniques to minimise environmental and public health issues. There are several techniques utilized, including photo-catalytic and electrochemical combined treatments, photo-catalytic degradation, sonochemical degradation, biodegradation, electrochemical degradation, adsorption process, chemical coagulation or flocculation, nano-filtration, oxidation, chemical precipitation, reverse osmosis, ozonation, ion-exchange, cloud point extraction, and ultra-filtration[11].

Adsorption, as contrasted with other techniques, may efficiently and adaptably remove colours from concentrated effluent. To remove contaminants from complicated matrices, adsorption is the utmost focused and efficient approach for water pollution treatment[12]. The progress of efficient noble adsorbents, such as activated carbon[13], zeolites[14], clay minerals[15], chitosan[16] and functionalized polymers[17] etc., has improved steadily over the past ten years. This is because the quality and cost-effectiveness of the adsorbent directly affect the efficiency of an adsorptive separation.

Unfortunately, most of these adsorbents have shown problems such as high cost, inefficiency (due to diffusion restriction or insufficient active surface sites), challenges with wastewater separation, or the production of secondary wastes. Recent literature review has shown that nano-adsorbents, such as waste-orange peel powder[18], *Citrus limon* wood waste[19] and litchi peel[20] exhibit great adsorption performance for the removal of metal ions. The solid-liquid separation issue often related with nanoparticles was successfully avoided by one such advanced type of adsorbent - magnetic nano-adsorbent with the help of an external magnetic field. High adsorption efficiency of the novel adsorbent is mainly due to its large surface to volume ratio and other unique properties, such as ease of synthesis, easy recovery and manipulation through subsequent coating and functionalization, lack of secondary pollutants, affordability, and environmental friendliness. Previous research on dyes removal from wastewater using activated carbon of walnut shell waste loaded with magnetized metallic oxide was lacking. In this work, walnut shell was used as precursors to create magnetic activated carbon to remove MO and MB dye from wastewater. The synthesis of carbon from walnut shell is low cast and simple experimental set-up and its efficiency can be activated by loading with magnetic Fe_2O_3. The adsorbent was characterised by FTIR, TEM, BET, SEM and EDX analysis. Using batch experiments, the impacts of contact duration, pH, and adsorbent dosage are evaluated to clear understand MWNSC ability to adsorb MO and MB dyes. To assess the adsorption procedure, equilibrium isotherms, kinetics, and thermodynamics for the adsorption of MO and MB on MWNSC are also established.

Experimental Section

Reagents

All reagents and chemicals used in the present study were of analytical grade without further purification. The 1 g of MOD and MBD were dissolved in 1 L of distilled water in a 1-L volumetric flask to yield a stock solution with a concentration of 1000 mg L^{-1}. The desired concentration of MOD and MBD was obtained by diluting the stock solution with distilled water. Using a pH meter (ELICO LI-120), a 0.1 M solution of NaOH and HCl was added to the solution to adjust its pH. Using a Perkin Elmer UV–visible spectrophotometer (Perkin Lambda 35), the concentration of the MO and MB dye solution was determined at 464 and 665 nm wavelengths.

Instrumentation

The newly prepared adsorbent was characterized using Fourier Transform Infrared (FT-IR) spectrometer (Shimadzu 84005 FT-IRS) to identify the functional groups. The porosity and specific surface area were calculated based on Brunauer, Emmett, and Teller (BET) model using a Thermo Surfer analyzer at liquid N_2 temperature of 77 K. A scanning electron microscope (SEM) linked to energy-dispersive X-ray spectroscopy (EDX) (JSM-6360LVSEM, JEOL Co., Japan) examined morphology and nanostructure synthetic materials. X-ray diffraction (XRD) studies were carried out by PANalytical X'Pert X-ray diffractometer to evaluate the crystallinity of the adsorbent.

Synthesis of raw walnut shell (WNS)

Walnut shells were gathered from local manufacturing industry in Salem, Namakkal, Tamil Nadu, India, and washed carefully with deionised water to remove dust particles and other impurities. The collected raw materials were exposed in sun light for 2 days and crushed into powder and stored in a bottle.

Synthesis of magnetic walnut shell based activated carbon (MWNSC)

About, 12 g of anhydrous ferric chloride ($FeCl_3$) and 6 g of hydrated ferrous chloride ($FeCl_2.6H_2O$) were mixed in 200 mL of distilled water and stirred vigorously at 80 °C for 30 min. Then 10 g of powered walnut shell was added and the solution was stirred for 1 h. Then 20 mL of 25% NaOH solution was

added in drop wise and stirring was continued until the black –coloured precipitate was obtained. The precipitate was filtered and dried at 100 ℃ for 12 h. The resultant impregnated samples were activated at 650 ℃ for 3 h in a muffle furnace. After cooling, the activated sample was washed with deionised water until the pH of the filtrate was about 6-7, and dried in a hot air oven for 6 h at 110 ℃. The decisive factors which determine the characteristic behaviour of the activated carbon could be pyrolyzed temperature, carbonization time and impregnation ratio. These factors could be maintained for the rich activation of walnut shell carbon. The obtained samples were named as magnetic walnut shell based activated carbon (MWNSC) and stored in a bottle then used for further experiments.

Adsorption process

The batch adsorption experiments were performed in 100 mL of the model solution containing a 100 mg L^{-1} concentration of the dye in a glass vessel. NaOH or diluted HCl were used to alter the pH of the solution. The pH studied ranged from 2 to 10. Thereafter, a pre-determined amount of the adsorbent (0.02–0.12 g) was mixed to the solution before sonication at ambient temperature for 15 –105 min. The supernatant was centrifuged and the amount of dye solution was estimated using a UV-visible spectrophotometer. The triplicate of each experiment was carried out, and the common values are reported in the work.

The amount of MO and MB adsorbed onto the sorbent was calculated using Eq. (1):

$$\text{Adsorption capacity } (q_e) = \frac{C_0 - C_e}{M} xV \quad \ldots(1)$$

where q_e is the amount of the adsorbate that was adsorbed in mg g^{-1}, C_o and C_e are the initial and equilibrium concentrations of dye in water after removal process (mg L^{-1}), respectively, V is the solution volume (L) and m is the amount of MWNSC material (g). The adsorption efficiency (% RE) was used as the analytical response using Eq. (2).

$$\% \text{ Removal efficiency} = \frac{C_0 - C_e}{C_0} x\ 100 \quad \ldots(2)$$

Finally, to ascertain the parameters of the adsorption response, kinetic and isotherm examinations were performed for each dye under optimal conditions. Adsorption isotherms were tested at starting dye concentrations of 40–200 mg L^{-1}, whereas kinetic assessments were executed by altering the exposure period from 15 to 120 min.

Adsorption isotherms

Adsorption isotherms were performed with 40-200 mg L^{-1} of dye solutions by adding 100 mg of adsorbent for 24 h at room temperature to reach equilibrium. The residual amount of dye solution was estimated by a UV-visible spectrophotometer. The adsorbed amount of MO and MB onto the adsorbent was calculated using Eq. (1).

The examination of isotherm data by fitting it into several isotherm models is a crucial step in determining the best model to employ for the design process. The experimental results were used to the two and three parameter non-linear isotherm models: namely Freundlich[21], Langmuir[22], Temkin[23], Redlich-Peterson[24], Sips[25], and Dubinin-Radushkevich[26].

Freundlich isotherm

The Freundlich isotherm is suitable for a highly heterogeneous surface and expressed by the following:

$$q_e = K_F C_e^{1/n} \quad \ldots(3)$$

Here, the Freundlich constant, denoted as K_F ((mg g^{-1})(L $mg^{-1})^{(1/n)}$), is associated with the bonding energy, while n (g L^{-1}) represents the adsorption's divergence from linearity.

Langmuir isotherm

The Langmuir model is obtained under the ideal assumption of totally homogenous adsorption surface and represented as follows:

$$q_e = \frac{q_m K_L C_e}{1 + K_L C_e} \quad \ldots(4)$$

where q_m (mg g^{-1}) is the maximum adsorption capacity for monolayer, and K_L (L mg^{-1}) Langmuir constant relating to adsorption energy.

Temkin isotherm

The Temkin and Pyzhev isotherm model includes an element that specifically takes into account adsorbate-adsorbing species interactions. According to this model, adsorbent-adsorbate interactions cause the heat of adsorption of all the molecules in the layer to decrease linearly with coverage. Adsorption is also characterized by a uniform distribution of binding energies up to a maximum binding energy. The Temkin isotherm has been employed in the following equation:

$$q_e = B \ln(AC_e) \quad ...(5)$$

where A (L mg^{-1}) is the state of equilibrium binding constant, which corresponds to the highest binding energy, and B is a Temkin constant associated with the heat of adsorption (kJ mol^{-1}).

Redlich-Peterson isotherm

The Redlich-Peterson isotherm is an empirical model with three parameters. It incorporates the Langmuir and Freundlich equations, and the adsorption mechanism is hybrid, rather than perfect monolayer adsorption. The equation for this model is given as:

$$q_e = \frac{K_R C_e}{1+a_R C_e^g} \quad ...(6)$$

where K_R (L g^{-1}) and a_R (L^g mg^{-1g}) are Redlich-Peterson isotherm constants and g is an exponent that lies between 0 and 1. For g=1, the equation converts to the Langmuir isotherm; for g=0, it simplifies to Henry's law equation; and for $1<<a_R C_e^g$, it is identical with the Freundlich isotherm.

Sips isotherm

The Sips isotherm is a hybrid expression that combines the Langmuir and Freundlich forms to anticipate heterogeneous adsorption systems and get around the Freundlich isotherm model's growing adsorbate concentration limit. It is possible to write it as follows:

$$q_e = q_{max}\frac{K_s C_e^{\gamma}}{1+K_s C_e^{\gamma}} \quad ....(7)$$

where q_{max} (mg g^{-1}) is the Sips maximum adsorption capacity, K_s (L mg^{-1}) the Sips equilibrium constant, and γ is the Sips model exponent.

Kinetic studies

It is critical to examine the adsorption rate and the time required for adsorption to achieve equilibrium. To understand and explore the adsorption mechanism, several empirical models may be employed to simulate the kinetics of solid-liquid interface adsorption[27]. In this case, the adsorption kinetics of MB and MO on MWNSC were predicted using pseudo-first order kinetic model[28], and pseudo-second order kinetic model [29] and Elovich[30].

The nonlinear forms of pseudo-first-order and pseudo-second-order equations are exposed in the following equation (8), (9) and (10), respectively.

$$q_t = q_e(1-e^{-k_1 t}) \quad ...(8)$$

$$q_t = \frac{k_2 q_e^2 t}{1+k_2 q_e t} \quad ...(9)$$

$$q_t = (1+\beta_E) \ln (1+\alpha_E \beta_E t) \quad ...(10)$$

where, k_1 and k_2 are the pseudo-first-order and second order constant; q_e and q_t are the sum of dye adsorbed at equilibrium and at time t.

Intra-particle diffusion study

The intraparticle diffusion coefficient (K_{id}) of MO and MB has been calculated at optimal initial dye concentrations and pH by employing the rate equation expressed by Weber and Morris[31] by the following equation:

$$K_{id} = \frac{q_t}{t^{1/2}} \quad ...(11)$$

where K_{id} is the rate constant for intraparticle diffusion (mg g^{-1} $min^{1/2}$), that can be measured from the slope of the linear plot of q_t vs. $t^{1/2}$.

Application to real dye wastewater

The dye wastewater samples were collected in the Tiruppur district in Tamil Nadu, India. About 500 mL of wastewater sample were kept in plastic bottles and under refrigeration at 4 to 8 °C. To avoid any possible contamination, polyethylene bottles were cleaned, placed in HNO_3 (1%) solution, and then washed with distilled water.

Results and Discussion

Adsorbent characterization

The presence of significant functional groups associated to the adsorbent can be determined using an excellent analytical instrument of Fourier transform infrared (FTIR) spectroscopy. FTIR spectroscopy is a useful method to study the interaction between an adsorbate and the functional groups which are active on the surface of the adsorbent. Both the porosity and the chemical reactivity of the functional groups at the surface affect the adsorption capacity of the adsorbent. Because of this reactivity, there is an imbalance between the forces within the body and at the surface, which causes the van der Waals force to adsorb molecules. Understanding surface functional groups would help one understand the adsorbent's capacity for adsorption. The FTIR spectrum of MWNSC before and after the adsorption of MO and MB loaded

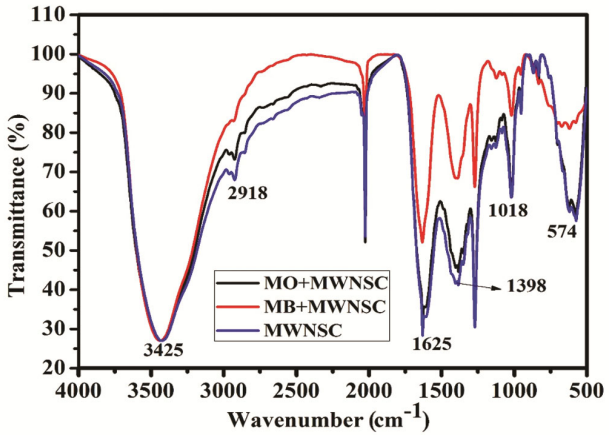

Fig. 1 — FTIR spectrum of MWNSC before and after the adsorption of MO and MB

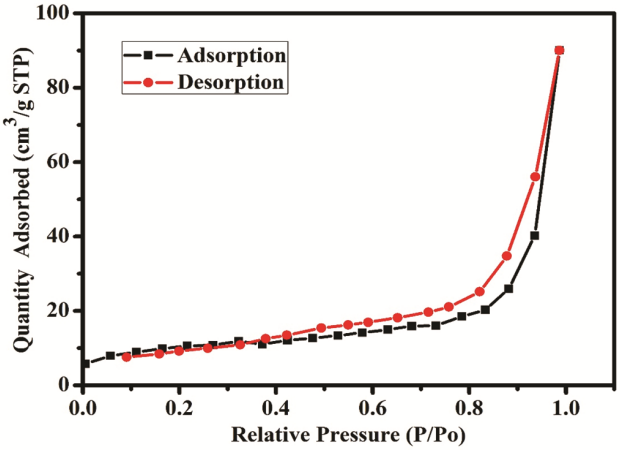

Fig. 2 — BET isotherm curve for MWNSC

MWNSC are picturized in Fig. 1. The stretching frequency of the O-H bond causes a significant peak at 3425 cm^{-1}, which confirms the existence of a hydroxyl group[32] in interaction with the type of hydrogen bond, whose structure corresponds to the residual presence of pectin, cellulose, hemicellulose and lignin, resulting from the process sample carbonization. The peak at 2918 cm^{-1} attributed to C-H bond stretching vibrations infers the existence of aliphatic groups (-CH_3 or –CH_2). The peaks at 1625 cm^{-1} might be consistent to the stretching of C= O in carboxyl groups[33]. The peak around 1398 cm^{-1} may be allocated to the symmetric stretching frequency vibration of –COO– group[34]. A faint peak of 1018 cm^{-1} was is attributed to stretches of glycosidic bonds (C-O) present in cellulose and hemicellulose. At the same time Fe-O group[30] was observed at a frequency of 574 cm^{-1}. After the MO and MB adsorption demonstrates that the position of the peaks were moved, some peaks vanished, and new peaks were found indicates that the participation of active functional groups present on the surface of MWNSC. It was observed that Fe^{2+}/O^{2-} interacts with charged MO (anionic) or MB (cationic) molecules, resulting in their adsorption on the surface of MWNSC.

The BET pore size, surface area, and pore volume distribution of prepared nanocomposites were analysed by BET analyser. The N_2 desorption isotherms curves of the MWNSC materials are depicted in Fig. 2. The BET surface area, pore volume, and pore diameter of MWNSC are found to be 126.27 $m^2 g^{-1}$, 0.224 cc g^{-1} and 3.28 nm, respectively. It ascribed to the available active sites on the adsorbent's surface that enhance the binding affinity of dye molecules. The adsorption of dye molecules is a surface phenomenon. Adsorption of dye molecules depends on surface functional groups, surface area and porosity of adsorbent. The porous structure (i.e., pore size and pore volume) and surface area contributed in the suitable binding sites for the dye adsorption[35, 36].The mesoporous structure and a huge specific surface area of MWNSC suggests a maximum adsorption capacity to the targeted adsorbates.

The structure and morphology of MWNNC were construed by TEM analysis and are shown in Fig. 3a. Internal structure and size of synthesized MWNNC nanocomposites were interpreted by TEM micrograph (Fig. 3a). Fig. 3a depict magnetic nanocomposites loaded activated carbon and their pore diameters are found to be around 18 nm. The Fe_2O_3 nanoparticles dispersed in pores of walnut shell carbon and it may decrease both the porosity and adsorbent's surface area. In fact, dye molecules adsorption is associated to surface area, porous structure and surface binding sites, the rate of adsorption decreases when Fe_2O_3 was loaded on MWNSC. The advantages of using Fe_2O_3 loading is the removal of MWNSC after adsorption of dyes. The morphology of MWNSC showed the existence highly mesoporous on the structure. The high mesoporous MWNSC has large active centres which increases the either physical or chemical interaction of dyes with the adsorbent.

The synthesised MWNSC had a porous structure and an irregular form, which improved their contact surface and the ability for MO and MB uptake, as seen by the SEM micrographs (Fig. 3b). Additionally, EDX attached with SEM apparatus was used to evaluate the chemical composition of the Fe_2O_3 loaded adsorbent (Fig. 3c). The EDX spectrum clearly shows the predictable elements including oxygen,

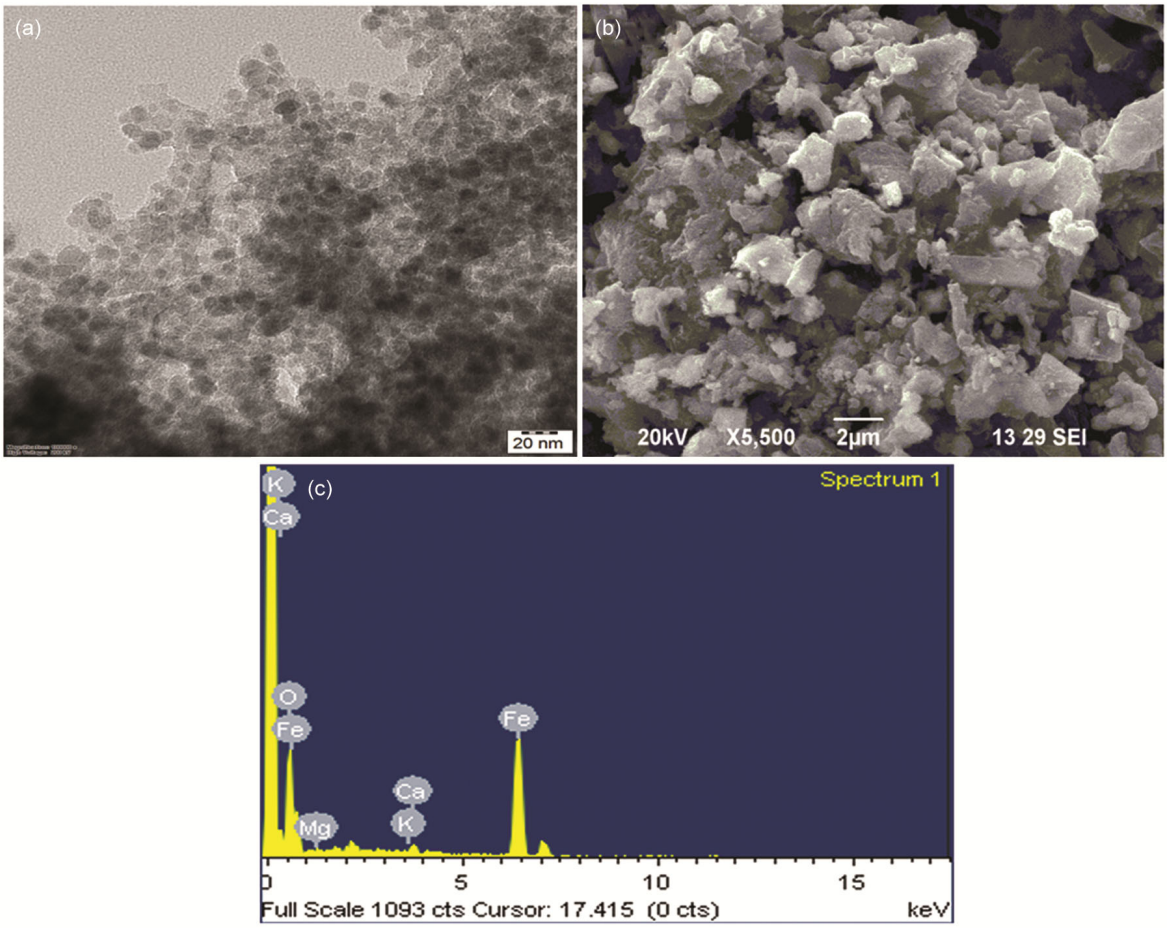

Fig. 3 — (a) TEM, (b) SEM and (c) EDX images of MWNSC

potassium, calcium, magnesium and iron. The presence of iron is corresponding to the magnetic Fe_2O_3 nanoparticles. These findings confirm the successful preparation of the green MWNSC adsorbent. Furthermore, the contents of Fe_2O_3 loaded in different regions on the MWNSC surface, which can also confirm that the adsorption of MB and MO onto the Fe_2O_3 loaded activated carbon is provided by surface reactions of iron oxide or hydroxide with MB and MO species forming complexes[37,38].

Primarily, alkali metal nitrates, such as potassium nitrate (0.01 N), are employed to calculate the zero charge. Fig. 4 depicts the findings of determining the point of zero charge for magnetic nanocomposites activated carbon (MWNSC). The pH_{pzc} values were used to determine the place where the resultant curves intersected the pH^0 axis, as illustrated in Fig. 4. This number can be used to forecast the surface charge of adsorbents; when adsorption occurs at a pH lower than the adsorbent's PZC, the adsorbent's surface

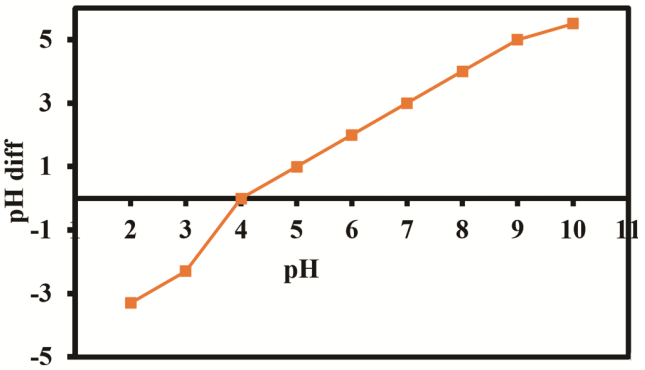

Fig. 4 — pH_{pzc} graph of MWMSC adsorbent

charge is positive, and when adsorption occurs above the PZC pH, the adsorbent's surface charge is negative. Fig. 4 shows the pH vs pH_{pzc} curve for the magnetic walnut shell.

An XPS measurement was conducted to further investigate the chemical nature of Fe_2O_3@MWNSC

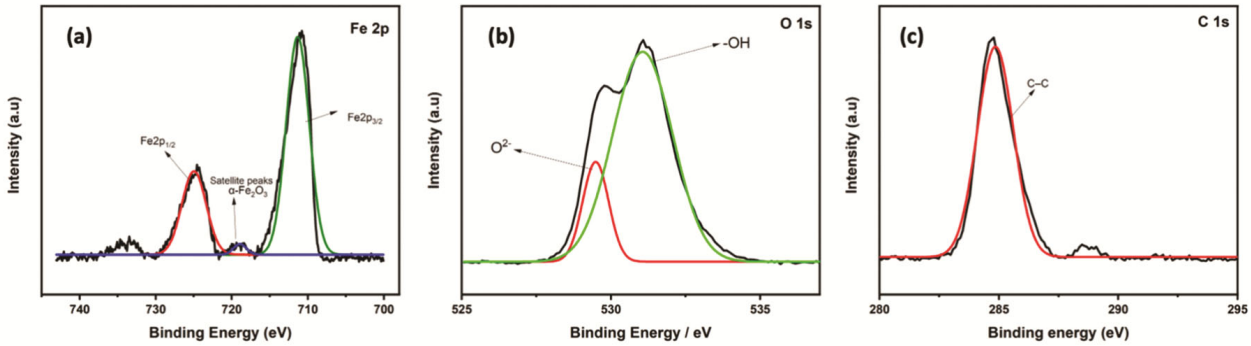

Fig. 5 — High resolution XPS profiles of (a) Fe 2p, (b) O 1s and (c) C 1s on MWNSC

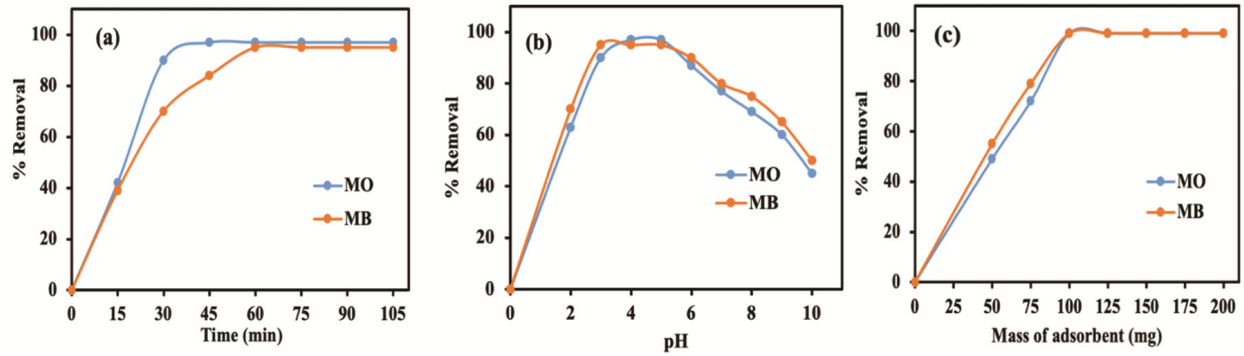

Fig. 6 — Effect of (a) contact time, (b) pH and (c) adsorbent mass

as prepared. In Fig. 5, graphs (a), (b) and (c) reveal a typical high resolution XPS spectrum in the Fe 2p region, and a typical O 1s and C 1s spectrum of Fe_2O_3 loaded MWNSC. On the surface, only the peaks associated with Fe, O, and C were exposed to the ambient atmosphere. As shown in Fig. 5(a), Fe_2O_3 has a core-level binding energy spectrum of Fe2p. There are peaks at 710.4 and 724.0 eV which correspond to Fe 2p3/2 and Fe 2p1/2, respectively. An additional satellite peak located at approximately 718.0 eV can be attributed to the Fe^{3+} state. In this illustration, a state +3 of Fe as Fe_2O_3 is loaded onto a walnut shell carbon layer. As shown in Fig. 5(b), the O 1s core-level spectrum has been fitted with two Gaussian peaks. It is likely that the peak at around 529.7 eV consists of O^{2-} in the Fe_2O_3 lattice. A second peak at 531.2 eV is likely caused by -OH group absorbed onto the surface of the Fe_2O_3 loaded MWNSC. In the O1s spectrum, two oxygen species are detected, which indicates oxygen enrichment on the surface[39,40]. On the deconvoluted spectrum of C 1s shown in Fig. 5(c), the peak at 284.5 eV is ascribed to the C-C bonds in the walnut shell activated carbon.

Evolution of adsorption characteristic of MWNSC

Adsorption experimental analysis

The equilibrium time is one of the key factors in the wastewater treatment process. Fig. 6(a) displays the outcomes of this study's investigation into the correlation between the removal effectiveness of MO and MB with contact time. According to Fig. 6(a) shows that the efficiency of adsorption increased with contact time and reached equilibrium after 60 and 45 min for MO and MB, respectively. The rapid adsorption at initial stage of contact time which is caused by increased the number of pores on the initial stage of MWNSC surface due to the faster mass transfer of the dyes from the solution onto the adsorbent. As a result, this suggests that the dyes have good accessibility to the binding sites on the adsorbent, which is favourable in the real world as it minimises the residence duration[41]. The optimal contact times were 60 and 45 min for MO and MB, respectively.

Solution pH is one of the most essential factors which affect the efficiency of the adsorbent on the surface charge and interaction between dye and active sites of the adsorbent. Fig. 6(b) shows that the removal efficiencies of the MO and MB dyes on the

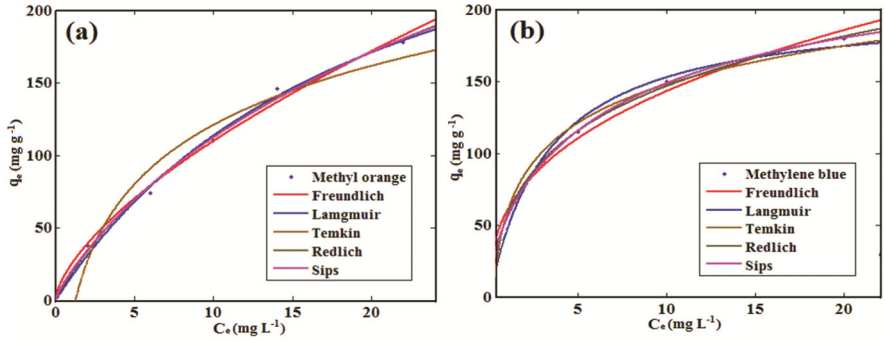

Fig. 7 — Nonlinear adsorption isotherm for (a) MO and (b) MB on MWNSC

MWNSC with changing the pH range of 2–10. It could be observed from the figure the removal efficiency of MO was highest at pH 2 (97 %) and significantly decreased with increasing pH from 97 - 30 %. On the other hand, the MB removal efficiency was decreased with increasing pH, attaining its extreme removal efficiency at pH 3 of 95 %. This is due to the fact that the pH values varied and altered the species of adsorbate in solution as well as the charge property of the adsorbent surface[42]. Fig. 6b presented that the functional groups of MWNSC would react with H^+ and get protonated when the value of pH is lower. The strong electrostatic attraction between the negatively charged MO and MB dyes and positively charged MWNSC surface made it easy for dyes to land on the adsorbent surface. Therefore, the adsorption capacity of MWNSC gets enhanced at low pH values. However, due to the increase of pH, the protonation on MWNSC surface gradually decreased. This led to the electrostatic repulsion between negatively charged adsorbent and MO/MB dyes, consequently decreasing the adsorption capacity. Furthermore, the interaction between adsorbent surface and dyes transformed to van der Waals force with the increment of pH value. The van der Waals force had a weaker effect compared to the electrostatic attraction, which resulted in the decrease of adsorption capacity. However, the quantity of OH^- ions enhanced with increasing pH, leading to competitive adsorption between OH^- and negatively charged dyes, so that the adsorption capacity gradually descended. The adsorption of OH^- could lead to the precipitation of metallic hydroxide on the surface of the adsorbent. Therefore, the following adsorption tests were performed at pH 3.0 for MO and 4.0 for MB to ensure the optimal adsorption capacity could be obtained.

It is essential to obtain the optimum adsorbent dose in order to completely exert the interactions between the adsorbate and adsorption sites. The effect on the removal efficiencies of the MO and MB dyes on MWNSC was evaluated by measuring the adsorbent mass (50 mg – 250 mg / 100 mL), contact time: 60 and 45 min for MO and MB, and dye concentration: 100 mg L^{-1} and optimum pH conditions for each dye. Fig. 6c demonstrates that as the adsorbent mass is changed from 50 mg to 100 mg, the efficiency of dye removal was significantly increased. This can be clarified by the increased in adsorbent's surface area and availability of adsorption sites[43]. The equilibrium and the maximum adsorption efficiency were attained for both dyes at 0.2 g, hence this value was chosen as the optimal mass of adsorbent condition for the subsequent research.

Adsorption isotherm analysis

An adsorption isotherm was used to analyse the mechanisms of the MO and MB dyes' interactions with the MWNSC adsorbent (Fig. 7a & b). The adsorption isotherm provides detailed information on the adsorption effectiveness of the adsorbent. The present study used the Langmuir, Freundlich, Temkin, Redlich and Sips isotherm adsorption models to characterise the MO and MB onto MWNSC.

The Langmuir isotherm adsorption model depicts the retention of adsorbent atoms (molecules, ions) in a monolayer on a uniform surface. The Temkin isotherm model is used to explain the direct relationship between surface inclusion and adsorption heat, while the model of Freundlich isotherm is used to illustrate multi-facet adsorption on an adsorbent with a heterogeneous surface[44]. The isotherm parameters listed in Table 1 shows that the MO and MB adsorption data are fit well with Langmuir isotherm model. This result essentially reflects the homogenous binding sites of the adsorbent's monolayer adsorption on the surface and the adsorption is uniformly distributed to all adsorption sites. The

Table 1 — Adsorption isotherm constants for MWNSC

Isotherm model	Parameters	MO	MB
Freundlich	K_F	24.85	60.57
	n (g L^{-1})	1.549	2.674
	SSE	138.5	149.7
	RMSE	6.794	7.063
	R^2	0.977	0.972
Langmuir	q_m(mg g^{-1})	345.70	303.30
	K_L (L mg^{-1})	0.049	0.305
	SSE	22.59	23.45
	RMSE	0.456	0.567
	R^2	0.997	0.995
Temkin	A (L mg^{-1})	0.7817	4.453
	B	25.53	16.73
	SSE	234.50	187.20
	RMSE	6.207	9.279
	R^2	0.968	0.965
Redlich-Peterson	K_R(L g^{-1})	21.60	140.80
	a_R(L mg^{-1})	1.173	1.597
	g	0.728	0.754
	SSE	108.4	183.4
	RMSE	7.513	6.413
	R^2	0.978	0.975
Sips	q_{max}(mg g^{-1})	427.2	244.4
	K_s (L mg^{-1})	0.024	0.063
	γ	0.821	0.525
	SSE	85.10	74.40
	RMSE	6.896	5.634
	R^2	0.972	0.977

monolayer adsorption capacity of MO and MB was 355.70 and 303.30 mg g^{-1}, respectively.

Table 2 summarises the elimination of MO and MB by various agricultural precursors. According to the literature review, adsorbents derived from various agricultural precursors exhibit a broad range of dye adsorption limits. This means that the examined MWNSC material was comparable from the literature is good, promising, and efficient for both MO and MB dyes from wastewater.

Kinetic adsorption studies

The adsorption mechanisms and potential rate-determining steps were investigated using a kinetic model. The kinetic behaviour of the MO and MB adsorption was investigated using pseudo-first-order, pseudo-second-order, Elovich and intraparticle diffusion kinetic models. Regression and data obtained from the kinetic study of the MO and MB adsorption are demonstrated in Fig. 8a, b and Table 2, respectively. According to the results, the data fitting to the pseudo-second-order model produced a strong correlation coefficient R^2, and the equilibrium adsorption capacity calculated by the model is more in line with the experimental values. Based on the findings, it can be revealed that the pseudo-second-order kinetic model offers a reliable connection for MO and MB adsorption by MWNSC. This observation revealed that chemical processes control the rate of dye adsorption. Cationic (MB and MO) dye molecules attract by electrostatic attraction to adsorbents with oppositely charged surface active binding sites, leading to chemisorption[55]. The intraparticle diffusion diagram of the adsorption of dyes by the adsorbent shows the regression line that failed to undergo the origin because C is not zero. This then counselled that each film and intraparticle diffusion affect the adsorption process.

Adsorption thermodynamic studies

Energy consideration is a crucial factor in determining the spontaneity of the process in adsorption chemistry. Thermodynamic parameter values indicate the practical applicability of a process.

Table 2 — Adsorption kinetic constants for MWNSC

Kinetic model	Parameters	MO	MB
Pseudo-first order	q_e,exp (mg g^{-1})	101.20	104.50
	k_1(min^{-1})	0.053	0.036
	q_e, cal (mg g^{-1})	116.70	128.90
	R^2	0.876	0.962
	SSE	238.1	234.9
	RMSE	6.298	6.257
Pseudo-second order	k_2 (g mg^{-1} min^{-1})	0.006	0.003
	q_e,cal (mg g^{-1})	102.10	103.7
	R^2	0.991	0.992
	SSE	14.86	12.86
	RMSE	0.564	0.765
Elovich	A	0.140	0.019
	B	8.352	12.71
	R^2	0.782	0.884
	SSE	441.5	396.2
	RMSE	8.578	8.126
Intraparticle- diffusion	K_{id} (g mg^{-1} min^{-1})	1.234	1.123
	C (mg g^{-1})	6.41	8.37
	R^2	0.682	0.784

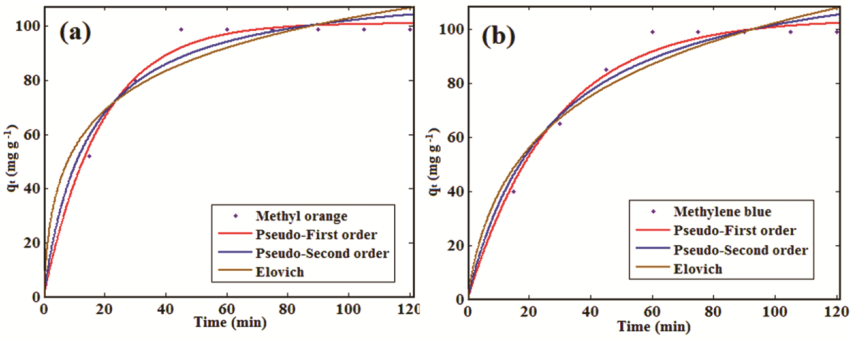

Fig. 8 — Nonlinear adsorption kinetics for (a) MO and (b) MB on MWNSC

The van't Hoff equation as follows

$$\ln K_c = \frac{\Delta S^0}{R} - \frac{\Delta H^0}{RT} \quad ...(12)$$

where K_c is the equilibrium rate constant which is the ration between the adsorbed dye concentration to that in solution. R is the gas constant (8.314 J mol^{-1} K) and T is the temperature in Kelvin. The free energy (ΔG^{o} / kJ mol^{-1}) can be measured using (ΔH^o/kJ mol^{-1}) and entropy (ΔS^o /kJ mol^{-1}). A graph of $\ln K_c$ versus 1/T should result a straight line that can be used to calculate (ΔH^o) and (ΔS^o) and ΔG^o. The thermodynamic parameters are shown in Table 3. The negative ΔH^o value indicates that the adsorption process is exothermic and the negative value of ΔS^o revealed that the decrease in randomness of dyes molecules caused by their adsorption on the surface of MWNSC. Finally, the negative ΔG^o values indicate that the MO and MB adsorption on MWNSC is spontaneous in nature.

Application for real wastewater sample

The samples of wastewater were collected from the dye industry in Tiruppur district in Tamil Nadu, India. The synthesised magnetic nanoparticles was utilised to remove MB and MO from real wastewater samples. The initial MO and MB concentration on real wastewater was found to be 25 and 30 mg L^{-1}. Table 4 shows that the prepared MWNSC adsorbent was able to remove MO and MB at greater than 99 % on real wastewater samples. Adsorbent regeneration and reuse potential is crucial for cost-effective and environmentally friendly water treatment methods. Not only should an exceptional adsorbent possess high adsorption efficiency, but it should also demonstrate productivity in

Table 3 — Thermodynamic parameters for the adsorption of MO and MB on MWNSC

Thermodynamic Parameters	Temperature (K)					
	MO			MB		
	300K	310K	320K	300K	310K	320K
ΔG^0 (kJ mol^{-1})	-11.329	-9.246	-7.153	-12.37	-8.57	-5.62
ΔH^0 (kJ mol^{-1})		-123.15			-126.40	
ΔS^0 (kJ mol^{-1} K^{-1})		-0.346			-0.447	

Table 4 — Application of MWNSC on the removal of MO and MB

Analyte	Initial conc. mg L^{-1}	Final conc. mg L^{-1}	% Removal
MO	25	0.080	99.7
MB	30	0.099	99.7

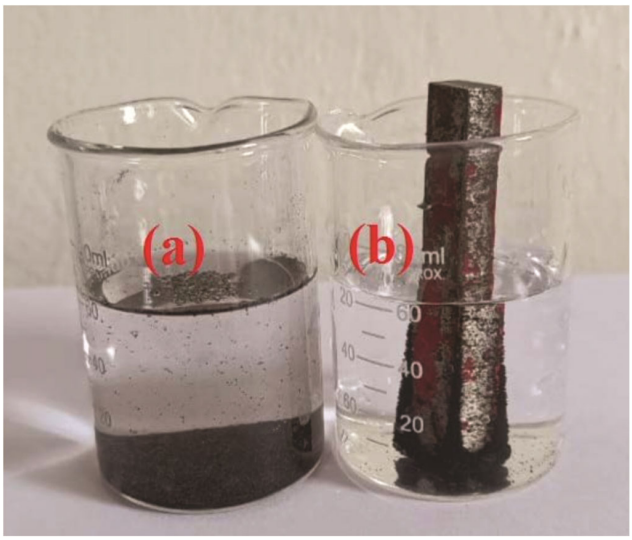

Fig. 9 — MWNSC particles in MO and MB solution, before (a) and after (b) magnetic separation

regeneration and reuse processes. By desorption method using desorbing solutions such as ethanol, methanol, HCl, NaOH, distilled water etc., the adsorbent MWNSC can be used in the real-world scenario.

Removal of MWNSC adsorbent from the dye solution

The solid–liquid separation process is crucial for the practical use of an adsorption process. A precisely measured 100 mg of MWNSC was dissolved in 10 mg·L^{-1} of dye solution in a 100 mL beaker. Sedimentation is the most basic technique for isolating solids from liquids. The process of removing adsorbents from homogenized MWNSC solutions in the absence and the presence of an external magnetic field is illustrated in Fig. 9. In the absence of an external magnetic field, the final sedimentation of MWNSC to the bottom takes 150 s. However, in the presence of an external magnetic field, the time required for MWNSC to completely separate was considerably reduced, to within 25 s. With an external magnetic field, this finding demonstrates that the magnetic adsorbent based on Fe_2O_3-coated walnut shell carbon can be extracted from solutions more quickly and easily than untreated adsorbents. Thus, these results are critical to the ongoing utilization and management of used adsorbents.

Table 5 — Monolayer adsorption capacities in the literature for MO and MB adsorption

Adsorbent	MO	MB
	q_m (mg g^{-1})	q_m (mg g^{-1})
Lotus leaf powder[39]	282.30	-
Anchote peel[40]	303.03	-
Moringaoleifera seed[41]	367.83	-
Cola nitida leaves[42]	527.84	530.41
Commercial activated carbon[43]	113.63	-
Orange peel[44]	-	98.90
Bamboo chip[45]		305.30
Nano activated carbon[46]	-	28.09
Jute stick powder[47]	-	37.89
Date pits[48]	434.0	555.0
MWNSC	**345.70**	**303.30**

Comparison with other adsorbents

Table 5 summarizes that the adsorption efficiency of MWNSC is compared with other adsorbents. The q_m value for MWNSC adsorbent showed 345.70 mg g^{-1} for MO and 303.30 mg g^{-1} for MB and revealed that it is one of the good adsorbent for the removal of MB and MO from the real wastewater. In comparison with other adsorbents, MWNSC has the advantage of a low cost of synthesis and a high adsorption efficiency of greater than 99%. The presence of the various functional groups such as -OH, -COO-, -C=O etc., are chemically interaction between MWNSC and dyes could be the reason for the high efficiency of adsorbent.

Adsorption mechanism

The mechanism of cationic dye adsorption is affected by various process parameters, including pH_{pzc}, pH of the solution, functional groups on the

surface, porosity of adsorbents, and dye type. Cationic dyes adhere to MWNSC by solid/liquid phase proximity, which might be electrostatic, hydrogen bonding, π-π interaction, or pore diffusion. MB and MO dyes were adsorbed onto the adsorbent via the following interaction and mechanism:

- Cationic dye molecules are electrostatically attracted to the negatively charged MWNSC nanocomposites. The negatively charged carboxyl (-COO$^{\cdot}$) and hydroxyl (OH^-) groups on the adsorbent surface interact with the cationic dye molecules at pH >pH_{pzc}.
- Dye adsorption onto an adsorbent also involves hydrogen bonding. When the adsorbent's pH <pH_{pzc}, the carboxyl (–COOH) group and water molecules on its surface may be presented with H–atoms to start a hydrogen bond with the polar N– or S–atoms of the MB and MO dye.
- The π-π interaction also controls the adsorption of cationic dye molecules onto the adsorbent. MWNSC is a material that has an aromatic structure with a C=C bond π-system. Through a π-π interaction, it interacted with the π-electron of the aromatic ring of MB and MO dye.
- The porous nature of MWNSC nanocomposite suggests that cationic dye molecules may be absorbed by pore diffusion or filling in addition to physical mechanisms.
- The functional groups of the adsorbent bound with the cationic dye molecules via hydrogen bonding, π-π interaction, and electrostatic contact, according to FTIR investigations of the adsorbent conducted before and after adsorption with cationic dyes.

Conclusion

The magnetically activated carbon derived from walnut shell by thermal activation, the mesoporous structure introduced by the co-precipitation method. The adsorbents were characterized by different analysis techniques to investigate their different physical and chemical characteristics. External physicochemical parameters that have a significant impact on the adsorption process include pH, temperature, competing compounds in solution, the type and polarity of the adsorbent and adsorbate, specific surface area, pore volume distribution, and so on. The results of the adsorption isotherm study indicate that the Langmuir is well-fitted with the experimental data. The adsorption capacity of MO and MB onto MWNSC was found to be as high as 345.70 and 345.70 mg g^{-1}, respectively, which is higher than a number of recently researched promising adsorbents. The kinetic investigation showed the adsorption process was well-fitted with a pseudo-second-order model. The thermodynamic study revealed that MO and MB adsorption using MWNSC follows a spontaneous and exothermic process. The maximum removal efficiencies of MO and MB dyes in wastewater samples was about 99%. Furthermore, the outcomes received shows that MWNSC nanocomposite could be a possible adsorbent for the adsorption process of MO and MB dyes. Therefore, magnetic walnut shell can be proposed as a potential low-cost adsorbent for the removal of organic dyes from coloured wastewater.

References

1 Jadhav J P, Kalyani D C, Telke A A, Phugare S S & Govindwar S P, Evaluation of the efficacy of a bacterial consortium for the removal of color, reduction of heavy metals, and toxicity from textile dye effluent, *Bioresour Technol*, 101 (2010) 165.

2 Basheer A A, Chemical chiral pollution: Impact on the society and science and need of the regulations in the 21st century, *Chirality*, 30 (2018) 402.

3 Alberti G, Amendola V, Pesavento M & Biesuz R, Beyond the synthesis of novel solid phases: Review on modelling of sorption phenomena, *Coord Chem Rev*, 256 (2012) 28.

4 Bai Y N, Wang X N, Zhang F, Wu J, Zhang W, Lu Y Z, Fu L, Lau T C & Zeng R J, High-rate anaerobic decolorization of methyl orange from synthetic azo dye wastewater in a methane-based hollow fiber membrane bioreactor, *J Hazard Mater*, 388 (2020) 121753.

5 Haque M M, Haque M A, Mosharaf M K & Marcus P K, Decolorization, degradation and detoxification of carcinogenic sulfonatedazo dye methyl orange by newly developed biofilm consortia, *Saudi J Biol Sci*, 28 (2021) 793.

6 Mahmood S, Khalid A, Arshad M, Mahmood T & Crowley D E, Detoxification of azo dyes by bacterial oxidoreductase enzymes, *Crit Rev Biotechnol*, 36 (2016) 639.

7 Wu L, Liu X, Lv G, Zhu R, Tian L, Liu M, Li Y, Rao W, Liu T & Liao L, Study on the adsorption properties of methyl orange by natural one-dimensional nano-mineral materials with different structures, *Sci Rep*, 11 (2021) 10640.

8 Alabbad E A, Efficient removal of methyl orange from wastewater by Polymeric Chitosan-*iso*-vanillin, *Open Chem J*, 7 (2020) 16.

9 Parlayıcı S & Pehlivan E, Biosorption of methylene blue and malachite green on biodegradable magnetic cortaderiaselloana flower spikes: Modeling and equilibrium study, *Int J Phytoremediation*, 23 (2021) 26.

10 Tunçsiper B, Combined natural wastewater treatment systems for removal of organic matter and phosphorus from polluted streams, *J Clean Prod*, 228 (2019) 1368.

11 Bharathi K S & Ramesh S T, Removal of dyes using agricultural waste as low-cost adsorbents: A review, *Appl Water Sci*, 3 (2013) 773.

12 Dai Y, Sun Q, Wang W, Lu L, Liu M, Li J, Yang S, Sun Y, Zhang K, Xu J, Zheng W, Hu Z, Yang Y, Gao Y, Chen Y,

Zhang X, Gao F & Zhang Y, Utilizations of agricultural waste as adsorbent for the removal of contaminants: A review, *Chemosphere*, 211 (2018) 235.

13 Huang X, Gao N Y & Zhang Q L, Thermodynamics and kinetics of cadmium adsorption onto oxidized granular activated carbon, *J Environ Sci*, 19 (2007) 1287.

14 Panuccio M R, Sorgonà A, Rizzo M & Cacco G, Cadmium adsorption on vermiculite zeolite and pumice: Batch experimental studies, *J Environ Manage*, 90 (2009) 364.

15 Hizal J & Apak R, Modeling of cadmium(II) adsorption on kaolinite-based clays in the absence and presence of humic acid, *Appl Clay Sci*, 32 (2006) 232.

16 Bamgbose J T, Adewuyi S, Bamgbose O & Adetoye A A, Adsorption kinetics of cadmium and lead by chitosan, *Afr J Biotechnol*, 9 (2010) 2560.

17 Panda G C, Das S K & Guha A K, Biosorption of cadmium and nickel by functionalized husk of Lathyrussativus, *Colloids Surf B*, 62 (2008) 173.

18 Gupta V K & Nayak A, Cadmium removal and recovery from aqueous solutions by novel adsorbents prepared from orange peel and Fe_2O_3 nanoparticles, *Chem Eng J*, 180 (2012) 81.

19 Peighambardoust S J, Foroutan R , Peighambardoust S H, Khatooni H & Ramavandi B, Decoration of citrus limon wood carbon with Fe_3O_4 to enhanced Cd^{2+} removal: A reclaimable and magnetic nanocomposite, *Chemosphere*, 282 (2021) 131088.

20 Jiang R, Tian J, Zheng H, Qi J, Sun S & Li X, A novel magnetic adsorbent based on waste litchi peels for removing Pb(II) from aqueous solution, *J Environ Manage*, 155 (2015) 24.

21 Freundlich H M F, Over the adsorption in solution, *J Phys Chem*, 57 (1906) 385.

22 Langmuir I, The adsorption of gases on plane surfaces of glass, mica and platinum, *J Am Chem Soc*, 40 (1918) 1361.

23 Temkin M J & Pyzhev V, Recent modifications to Langmuir isotherms, *Acta Physicochim*, *Acta Physiochim*, 12 (1940) 217.

24 Redlich O & Peterson D L, A useful adsorption isotherm, *J Phys Chem*, 63 (1959) 1024.

25 Sips R, On the structure of a catalyst surface, *J Phys Chem*, 16 (1948) 490.

26 Dubinin M M & Radushkevich L V, Equation of the characteristic curve of activated charcoal, *Chem Zent*, 1 (1947) 875.

27 Simonin J P, On the comparison of pseudo-first order and pseudo-second order rate laws in the modeling of adsorption kinetics, *Chem Eng J*, 300 (2016) 254.

28 Sudha R, Srinivasan K & Premkumar P, Removal of nickel(II) from aqueous solution using *Citrus limettioides* peel and seed carbon, *Ecotoxicol Environ Saf*, 117 (2015) 115.

29 Ho Y S & Ofomaja A E, Pseudo-second-order model for lead ion sorption from aqueous solutions onto palm kernel fiber, *J Hazard Mater*, 129 (2006) 137.

30 Sribharathi S, Sudha R, Anitha P, Poornima K & Kavitha G, Cadmium(II) removal from aqueous solution using a novel magnetic nanoparticle impregnated onto *Citrus hystrix* leaves, *Desal Water Treat*, 196 (2020) 388.

31 Weber W J & Morris J C, Kinetics of adsorption on carbon from solution, *J Sanit Eng Div*, 89 (1963) 31.

32 Sribharathi S, Kavitha G & Sudha R, Synthesis of magnetic activated carbon from *Citrus hystrix* leaves with excellent Pb(II) adsorption performance towards electroplating wastewater, *Ind J Chem Technol*, 29 (2022) 229.

33 Vaithianathan R, Anitha P, Ramachandran A & Sudha R, A green synthesis of Fe_3O_4 nanocomposites loaded castor seed shell carbon for lead(II) removal from water: Equilibrium and kinetic studies, *Desal Water Treat*, 280 (2022) 271.

34 Chen J, Gao Y C, Xu Z B, Wu G H, Chen Y C & Zhu C Q, A novel fluorescent array for mercury (II) ion in aqueous solution with functionalized cadmium selenide nanoclusters, *Anal Chim Acta*, 577 (2006) 77.

35 Bora P, Bhuyan C, Borah A R & Hazarika S, Carbon nanomaterials for designing next-generation membranes and their emerging applications, *Chem Commun*, 59 (2023) 11320.

36 Gogoi M, Goswami R, Borah A & Hazarika S, In situ assembly of functionalized single-walled carbon nanotube with partially reduced graphene oxide nanocomposite membrane for chiral separation of β-substituted-α-amino acids, *Sep Purif Technol*, 283 (2022) 120201.

37 Gogoi M, Goswami R, Ingole P G & Hazarika S, Selective permeation of L-tyrosine through functionalized single-walled carbon nanotube thin film nanocomposite membrane, *Sep Purif Technol*, 233 (2020) 116061.

38 Gogoi M, Goswami R, Borah A, Sarmah H, Rajguru P & Hazarika S, Amide functionalized DWCNT nanocomposite membranes for chiral separation of the racemic DOPA, *Sep Purif Technol*, 279 (2021) 119704.

39 Borah A, Gogoi M, Goswami R, Sarmah H, Hazarika K K & Hazarika S, Thin film nanocomposite membrane incorporated with clay-ionic liquid framework for enhancing rejection of epigallocatechin gallate in aqueous media, *J Environ Chem Eng*, 10 (2022) 107423.

40 Bhuyan C, Konwar A, Bora P, Rajguru P & Hazarika S, Cellulose nanofiber-poly (ethylene terephthalate) nanocomposite membrane from waste materials for treatment of petroleum industry wastewater, *J Hazard Mater*, 442 (2023) 129955.

41 Zhao W, Zhao Y, Zhang H, Hao C & Zhao P, Efficient removal of cationic andanionic dyes by surfactant modified Fe_3O_4 nanoparticles, *Colloids Surf A*, 633 (2022) 127680.

42 Tanhaei B, Ayati A, Lahtinen M & Sillanpaa M, Preparation and characterization of a novel chitosan/Al_2O_3/magnetite nanoparticles composite adsorbent for kinetic, thermodynamic and isotherm studies of methyl orange adsorption, *Chem Eng J*, 259 (2015) 1.

43 Argun M E, Guclu D & Karatas M, Adsorption of reactive blue 114 dye by using a new adsorbent: Pomelopeel, *J Ind Eng Chem*, 20 (2014) 1079.

44 Cheng S, Zhao S, Xing B, Liu Y, Zhang C & Xia H, Preparation of magnetic adsorbent-photocatalyst composites for dye removal by synergistic effect of adsorption and photocatalysis, *J Clean Prod*, 348 (2022) 131301.

45 Munagapati V S, Wen H Y, Gollakota A R K, Wen J C, Shu C M, Lin K Y A, Yarramuthi V, Wen J H, Reddy G M & Zyryanov G V, Enhanced removal of anionic methyl orange azo dye by an iron oxide (Fe_3O_4) loaded lotus leaf powder (LLP @ Fe_3O_4) composite synthesis, characterization, kinetics, isotherms and thermodynamic perspectives, *Inorg Chem Commum*, 151 (2023) 110625.

46 Hambisa A A, Regasa1 M, Ejigu H G & Senbeto C B, Adsorption studies of methyl orange dye removal from aqueous solution using anchote peel-based agricultural waste adsorbent, *Appl Water Sci*, 13 (2023) 24.

47 Raji Y, Nadi A, Rouway M, Sbai S J, Yassine W, Elmahbouby A, Cherkaoui O & Zyade S, Efficient adsorption of methyl orange on nanoporous carbon from agricultural wastes: Characterization, kinetics, thermodynamics, regeneration and adsorption mechanism, *J Compos Sci*, 6 (2022) 385.

48 Mbachu C A, Babayemi A K, Egbosiuba T C, Ike J I, Ani I J & Mustapha S, Green synthesis of iron oxide nanoparticles by Taguchi design of experiment method for effective adsorption of methylene blue and methyl orange from textile wastewater, *Results Eng*, 19 (2023) 101198.

49 Khattabi E H E L, Rachdi Y, Bassam R, Mourid E H, Naimi Y, Alouani M E L & Belaaouad S, Enhanced elimination of methyl orange and recycling of an eco-friendly adsorbent activated carbon from aqueous solution, *Russ J Phys Chem*, 15 (2021) 149.

50 Gurer A G, Aktas K, Akcetin M O, Unsar A E & Asilturk M, Adsorption isotherms, thermodynamics, and kinetic modeling of methylene blue onto novel carbonaceous adsorbent derived from bitter orange peels, *Water Air Soil Pollut*, 232 (2021) 138.

51 Jawad A H & Abdulhameed A S, Statistical modeling of methylene blue dye adsorption by high surface area mesoporous activated carbon from bamboo chip using KOH-assisted thermal activation, *Energy Ecol Environ*, 5 (2020) 456.

52 Shokry H, Elkady M & Hamad H, Nano activated carbon from industrial mine coal as adsorbents for removal of dye from simulated textile wastewater: Operational parameters and mechanism study, *J Mater Res Technol*, 8 (5) (2019) 4477.

53 Nipa S T, Rahman M W, Saha R, Hasan M M & Deb A, Jute stick powder as a potential low-cost adsorbent to uptake methylene blue from dye enriched wastewater, *Desal Water Treat*, 153 (2019) 279.

54 Mahmoudi K, Hosni K, Hamdi N & Srasra E, Kinetics and equilibrium studies on removal of methylene blue and methyl orange by adsorption onto activated carbon prepared from date pits-a comparative study, *Korean J Chem Eng*, 32 (2015) 274.

55 Baruah K, Bhattacharyya P K & Hazarika S, Adsorption of dilute alcohols onto cyclodextrin polysulfone membrane: Experimental and theoretical analysis, *J Chem Eng Data*, 60 (2015) 2549.